Journal of Engineering Mathematics **44:** 311–330, 2002.

Exact solutions for two steady inviscid bubbles in the slow viscous flow generated by a four-roller mill

DARREN CROWDY
Department of Mathematics, Imperial College of Science, Technology and Medicine, 180 Queen's Gate, London, SW7 2BZ, U.K. (e-mail: d.crowdy@ic.ac.uk)

Received 17 May 2002; accepted in revised form 29 August 2002

Abstract. The nonlinear free-boundary problem of finding the equilibrium shapes of two equal-sized two-dimensional inviscid bubbles with surface tension situated in a polynomially-singular slow viscous flow is solved in terms of closed-form formulae. The singular flow is taken to be within the class of those realizable at the centre of a four-roller mill apparatus. The associated flow field is also found explicitly. These solutions allow investigation of the bubble shapes and associated streamline patterns as functions of the far-field asymptotic conditions. In certain regimes, the bubbles are found to exhibit both near-cusps and a characteristic dimpling as they draw closer together. The results provide the first instances of exact solutions involving two interacting bubbles in an unbounded Stokes flow.

Key words: bubbles, Stokes flow, surface tension.

1. Introduction

The problem of interaction of multiple bubbles and fluid droplets dispersed in a second host fluid is important in many industrial applications. Processes such as droplet coalescence can only be understood by studying the interaction between two or more droplets. Chesters [1] provides a comprehensive review of this area. The converse scenario is breakup, where a single bubble or droplet evolves to a situation involving multiple bubbles/droplets. The deformation and breakup of drops and bubbles is relevant to such physical processes as the rheology of emulsions and mixing in multiphase systems. An early review of this area is provided by Rallison [2] and a more recent one by Stone [3].

Difficulties in resolving the hydrodynamic interaction of two droplets or bubbles (and hence flows involving two disjoint free surfaces) have resulted in very few theoretical or mathematical results in the literature concerning bubble interaction in an ambient flow field. Analytical solutions to a fully three-dimensional situation still prove elusive owing to a lack of suitable mathematical techniques. On the other hand, simplified two-dimensional models of free-surface Stokes flow can be tackled by complex-variable methods. A variety of such results have been established (*e.g.* [4]–[16]). Moreover, from a physical point of view, these two-dimensional solutions shed light on important qualitative aspects of axisymmetric flows. Antanovskii's analytical solutions [10], [11] for cusping bubbles, for example, have striking similarities with the three-dimensional bubbles observed in Taylor's early experiments in a four-roller mill [17].

To the best of this author's knowledge, no analytical results for the problem of *two* interacting bubbles in an unbounded ambient Stokes flow currently exist in the literature. An exception is recent work by the present author in which exact solutions are found for multiple

time-evolving bubbles in *bounded* Stokes flows [16]. The present paper makes a contribution in this direction by deriving a class of explicit solutions for the equilibrium shapes of two inviscid bubbles placed in a polynomially-singular flow typical of that produced at the centre of a four-roller mill.

This paper has been inspired by two prior investigations. The first is recent experimental work on the problem of two-droplet coalescence. Yang *et al*. [18] have studied experimentally velocity-gradient-induced coalescence at the individual droplet level, *i.e.*, the coalescence of two equal-sized droplets in a linear ambient flow. These experiments were carried out using a linear flow produced in a four-roller mill apparatus. The second source of motivation is the known existence of classes of exact solution for a *single* constant-pressure bubble in an ambient Stokes flow typical of that produced in a four-roller mill. Using boundary-integral calculations, Antanovskii [11] deduced the form of the local flow in the neighbourhood of a small bubble at the centre of the four-roller mill constructed by Taylor [17] in his classic early experiments. Working in the spirit of matched asymptotic expansions, Antanovskii [11] used the local expansion of this numerical 'outer' solution as the far-field boundary conditions for an 'inner' free-boundary problem. This inner problem was solved using complex-variable methods to find the shape of the bubble, and the associated flow field, in closed form. These complex-variable methods were first developed in Antanovskii [10] for far-field flows within the same class. The ambient 'outer' flows of Antanovskii [10], [11] have the form of a purely straining orthogonal stagnation-point flow. Pozrikidis [19], [20] has studied time-evolving bubbles in this class of ambient flows using boundary-integral methods. Later, Siegel [21] found exact solutions to the same (time-dependent) problem considered by Pozrikidis [19], however, such exact solutions only exist provided the bubble area remains constant in time (see Crowdy and Siegel [22] for clarification of this point).

This paper extends the second part of Antanovskii's analysis to the case of two symmetric bubbles placed in the same class of outer ambient flows considered in [10], [11]. The present analysis is therefore a generalization to the case of two interacting bubbles of the steady single-bubble analysis of Antanovskii [10], [11]. The latter work is itself a natural generalization of earlier investigations by Richardson who identified exact solutions for the equilibrium shapes of a single bubble both in linear flows [4] and parabolic flows [5].

This paper focuses on presenting details of the mathematical solutions and in exploring their properties. The solutions fully resolve the global bubble deformation due to the ambient flow and the interaction effects due to the presence of a second bubble. Closed-form formulae for the free-surface shapes and the associated flow field are found for different ambient flow conditions.

It is anticipated that one of the more important roles of the exact solutions will be to provide non-trivial checks on numerical codes (*e.g.*, boundary integral codes) written to resolve the more general unsteady evolution of two bubbles in a two-dimensional ambient flow. Moreover, theoretical treatment of two-bubble interactions involves mostly asymptotic and/or perturbative procedures. For example, the droplet-coalescence problem is usually analysed by first resolving the mutual approach of the bubbles under the effects of the ambient flow then, once the bubbles are close enough, some inner asymptotic (usually 'thin film') analysis of film drainage is performed. In this spirit, the present results might serve as leading-order solutions in theoretical treatments where additional effects are introduced perturbatively.

In Section 2, a complex-variable formulation of the problem is presented. In Section 3, the choice of the class of far-field boundary conditions is discussed. In Sections 4–5, the analysis leading to the solutions is presented, while Section 6 presents details of the resulting solutions.

Finally, the paper concludes with a discussion of possible generalizations and application of the results.

2. Mathematical formulation

The model problem treated here is idealized in that the flow is assumed to be two-dimensional, the two bubbles are assumed to be of equal size and of constant interior pressure and the ambient flow is taken to be a slow viscous Stokes flow with a far-field behaviour typical of that produced in a four-roller mill apparatus.

Consider two equal-sized plane inviscid bubbles placed in an infinite region D occupied by a very viscous fluid of viscosity μ in the Stokes regime. Because the flow is incompressible, a streamfunction $\psi(x, y)$ is introduced such that

$$\mathbf{u} = (u, v) = (\psi_y, -\psi_x), \tag{1}$$

and which satisfies the biharmonic equation in the fluid region (see [23], *i.e.*,

$$\nabla^4 \psi = 0 \quad \text{in } D. \tag{2}$$

It is further assumed that the two bubbles are symmetric in the sense that each is a rotation about the origin by an angle π of the other. The internal bubble pressures are assumed equal and, without loss of generality, set equal to zero. A uniform surface tension σ acts on each bubble boundary and is assumed to be the same for both. The equation of stress balance on each bubble boundary takes the form

$$-pn_j + 2\mu e_{jk} n_k = \sigma \kappa n_j, \tag{3}$$

where p is the fluid pressure, e_{jk} is the fluid rate-of-strain tensor and κ is the surface curvature. n_i denotes the i-th component of the vector normal to the boundary. The kinematic condition on the bubble boundaries in the steady case requires that each surface is a streamline (*i.e.*, a ψ-contour). It will also be necessary to impose boundary conditions on the flow at infinity as described in detail in Section 3.

The general solution of (2) can be written, in terms of the usual complex variable $z = x + \mathrm{i}y$ and its complex conjugate $\bar{z} = x - \mathrm{i}y$, as

$$\psi = \mathfrak{Im}[\bar{z} f(z) + g(z)], \tag{4}$$

where $f(z)$ and $g(z)$ are analytic in the fluid region D except at infinity where they exhibit the singular behaviour to be described in Section 3. The following relations can be established [23, pp. 156–160]:

$$\frac{p}{\mu} - \mathrm{i}\omega = 4f'(z), \quad u + \mathrm{i}v = -f(z) + z\bar{f}'(\bar{z}) + \bar{g}'(\bar{z}), \quad e_{11} + \mathrm{i}e_{12} = z\bar{f}''(\bar{z}) + \bar{g}''(\bar{z}), \tag{5}$$

where $\omega = -\nabla^2 \psi$ is the vorticity of the fluid. The conjugate function $\bar{f}(z)$ is defined as

$$\bar{f}(z) = \overline{f(\bar{z})}. \tag{6}$$

It is convenient to non-dimensionalize velocities by σ/μ, pressure by σ/a_0 and length and time by a_0 and $a_0\mu/\sigma$, where a_0 is a typical length scale of the bubbles. It is assumed that one bubble is situated on the negative real axis, while bubble 2 is situated on the positive real axis. Upon defining s to be the arclength traversed in a clockwise direction around each bubble boundary, the stress condition on bubble 1 takes the form

$$f(z) + z\bar{f}'(\bar{z}) + \bar{g}'(\bar{z}) = -i\frac{z_s}{2} + A_1, \tag{7}$$

where A_1 is a constant of integration and $z_s = \mathrm{d}z/\mathrm{d}s$. See, for example, Crowdy and Tanveer [12] for a derivation of this result. Similarly, the stress boundary condition on bubble 2 is

$$f(z) + z\bar{f}'(\bar{z}) + \bar{g}'(\bar{z}) = -\mathrm{i}\frac{z_s}{2} + A_2, \tag{8}$$

where A_2 is another integration constant. The kinematic condition on each bubble boundary can be written as

$$\Im\mathrm{m}\,[(u + \mathrm{i}v)\bar{z}_s] = 0. \tag{9}$$

The constants A_1 and A_2 in (7) and (8) are determined implicitly by the bubble shapes (see [4], [14] for a discussion of this point) and are not directly related to the interior bubble pressures. It can be seen from (5) that $f(z)$ and $g'(z)$ are only determined up to additive degrees of freedom; transforming $f(z) \mapsto f(z) + A$ and $g'(z) \mapsto g'(z) + \bar{A}$ where A is some constant, can be seen not to affect either the fluid pressure, velocity or stress fields. This degree of freedom implies that one of the constants in (7) and (8) can be specified to be zero. The symmetry of the bubble configuration also constrains these constants of integration. To see this, consider a transformation corresponding to a rotation of the flow domain by an angle π so that the set $\{z, f(z), g(z), A_1, A_2\}$ maps to the set $\{\mathcal{Z}, \mathcal{F}(\mathcal{Z}), \mathcal{G}(\mathcal{Z}), \mathcal{A}_1, \mathcal{A}_2\}$. Inspection of the formulae in (5) for the pressure and velocity fields implies that z and the two Goursat functions must transform as follows:

$$\mathcal{Z} = -z, \quad \mathcal{F}(\mathcal{Z}) = -f(z), \quad \mathcal{G}'(\mathcal{Z}) = -g'(z). \tag{10}$$

Using (10) in the stress condition implies that the constants A_j transform as

$$\mathcal{A}_j = -A_j, \qquad j = 1, 2. \tag{11}$$

However, because the domain is invariant under a rotation through π, then in order that the stress boundary conditions be similarly invariant, we take $A_1 = A_2 = 0$.

3. The flow-field induced by a four-roller mill

It is assumed that the only singularity of the flow exterior to the two bubbles occurs at infinity. The conditions on $f(z)$ and $g(z)$ as $z \to \infty$ are taken to be of the polynomial form

$$f(z) \sim f_3 z^3 + f_1 z + \dots, \quad g(z) \sim g_4 z^4 + g_2 z^2 + \dots, \tag{12}$$

where f_3, f_1, g_4 and g_2 are constants. Using the expressions for the physical quantities in terms of the Goursat functions given in (5), we may easily deduce that the expansions (12) are the only ones consistent with the required symmetries of the problem. In the far-field, both the fluid velocities and fluid pressure associated with (12) are divergent. The choice (12) coincides with the class of rotational far-field flows considered in the case of a single bubble by Antanovskii [10] in his analysis to demonstrate analytically the formation of a cusped bubble in a four-roller mill. Later, using boundary-integral methods based on the configuration used in Taylor's original experiments, Antanovskii [11] showed that the behaviour of $f(z)$ and $g(z)$, as stated in (12) for specific choices of parameters g_4, g_2, f_3 and f_1, includes the small $|z|$ expansion of the 'outer' flow generated by the rollers in the mill. In the spirit of matched

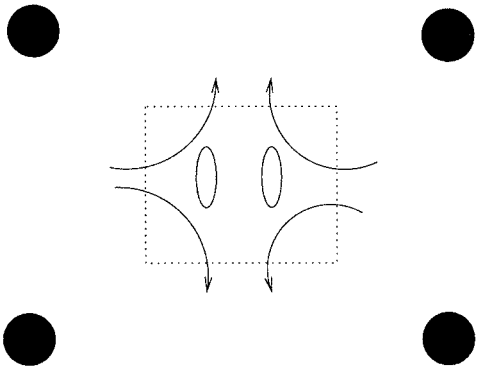

Figure 1. Schematic of the problem under consideration. Two bubbles are placed at the centre of a four-roller mill. The bubbles are assumed small compared to the size of the mill. The problem considered is the 'inner' free boundary problem (localized in the dotted rectangle) which must be matched to a polynomially-singular far-field flow (*cf*: (12)) given by the local expansion (near the mill centre) of the 'outer flow' produced by the four rollers (shown as darkly-shaded circles).

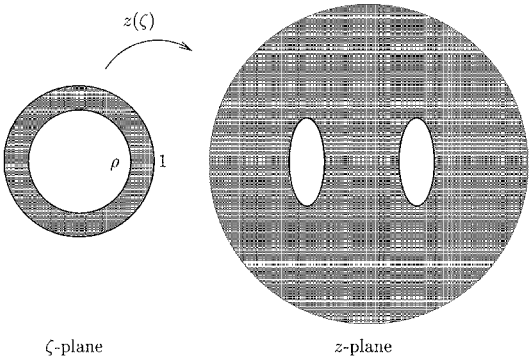

Figure 2. Conformal mapping domains. The shaded annulus $\rho < |\zeta| < 1$ maps in a one-to-one fashion onto the unbounded (shaded) exterior of the two bubbles.

asymptotic expansions, the 'inner' problem of flow induced around a small bubble at the centre of the mill must therefore match to the boundary conditions (12) in the far-field. This inner flow problem is solved exactly [11] using complex-variable methods.

This paper follows this idea but includes the additional feature that there are now two bubbles at the centre of the mill. It is again assumed that both bubbles are much smaller than the typical size of the mill so that a local expansion of the 'outer' flow due to the four rollers provides the far-field flow (12) to which the 'inner' flow must be matched. Figure 1 provides a schematic of the inner free-boundary problem to be solved. It will be solved here by generalizing the methods employed by Antanovskii [10] – a generalization that is nontrivial because the fluid region is now an unbounded, doubly-connected region with two separate free surfaces over which all boundary conditions must be simultaneously satisfied.

To assign physical significance to the constants f_3, f_1, g_4 and g_2 we follow an argument of Antanovskii [10]. To understand the expansion of the irrotational component $g(z)$, observe that the complex velocity potential $w(z)$ associated with a simple model of the four-roller mill configuration in which four vortices of opposite but equal strength Γ are placed at positions $\{c, \bar{c}, -c, -\bar{c}\}$ (where $c = c_x + \mathrm{i}c_y$) is given by

$$w(z) = -\frac{\mathrm{i}\Gamma}{2\pi} \log\left(\frac{1 - z^2/c^2}{1 - z^2/\bar{c}^2}\right). \tag{13}$$

If the average radius of a bubble at the centre of the mill is much less than $|c|$, the leading-order expansion for $w(z)$ is

$$w(z) \sim -\frac{2\Gamma c_x c_y}{\pi |c|^4} z^2 - \frac{2\Gamma c_x c_y (c_x^2 - c_y^2)}{\pi |c|^8} z^4 + \dots, \tag{14}$$

and (14) constitutes the far-field conditions for an inner problem governing the shapes of the bubbles. We can therefore make the identification

$$g_2 = -\frac{2\Gamma c_x c_y}{\pi |c|^4}, \quad g_4 = -\frac{2\Gamma c_x c_y (c_x^2 - c_y^2)}{\pi |c|^8}. \tag{15}$$

The constants g_2 and g_4 thus depend on the geometry of the mill and the rate of rotation of the rollers. g_2 can be associated with the strength of a local stagnation-point flow at the centre of the mill and might be measured experimentally by determining the velocity gradient along the centreline of the mill. In Taylor's experiments the rollers were positioned at the four corners of a square so that $g_4 = 0$ (this is consistent with (15) if $c_x = c_y$). In more general mill configurations with rollers placed at the corners of a general rectangle (so that $c_x \neq c_y$) g_4 will be non-zero. For maximal generality, we treat the general class of far-field conditions (12) with no special restrictions imposed on the mill configuration (that is, we allow for a non-zero g_4). As corroborated by the boundary-integral calculations of Antanovskii [11], the Stokes flow generated at the centre of a four-roller mill is not purely irrotational and there is a rotational component associated with non-zero $f(z)$. Inspection of (5), shows that the constants f_3 and f_1 are associated with pressure gradients.

4. Steady solutions

Setting $A_1 = A_2 = 0$ and combining (7)–(9), we may show that the kinematic condition (9) on the free surface of both bubbles is equivalent to

$$-\Im\mathrm{m}\left[2f(z)\bar{z}_s\right] = \frac{1}{2}. \tag{16}$$

Defining $W(z, \bar{z}) = \bar{z} f(z) + g(z)$, we have on each free surface,

$$\frac{\mathrm{d}W}{\mathrm{d}s} = \frac{\partial W}{\partial z} z_s + \frac{\partial W}{\partial \bar{z}} \bar{z}_s = (\bar{z} f'(z) + g'(z)) z_s + f(z)\bar{z}_s. \tag{17}$$

From the stress conditions,

$$\bar{z} f'(z) + g'(z) = \mathrm{i}\frac{\bar{z}_s}{2} - \bar{f}(\bar{z}) \tag{18}$$

on both bubble surfaces, so

$$\frac{\mathrm{d}W}{\mathrm{d}s} = \frac{\mathrm{i}}{2} + \mathrm{i}\,\Im\mathrm{m}[2f(z)\bar{z}_s] = \mathrm{i}\left(\Im\mathrm{m}[2f(z)\bar{z}_s] + \frac{1}{2}\right) = 0, \tag{19}$$

where the last equality follows from (16). It follows that W is constant on each bubble boundary, *i.e.*,

$$\begin{aligned} W &= C_1, \quad \text{on bubble 1;} \\ W &= C_2, \quad \text{on bubble 2.} \end{aligned} \tag{20}$$

Without loss of generality, we set $C_1 = 0$. By the imposed symmetry of the configuration, we expect $C_2 = 0$ and seek solutions where $W = 0$ on both bubble boundaries.

5. Conformal mapping

The fluid region in the two-bubble case considered here is an unbounded doubly-connected domain. To reconstruct the fluid domains, it is convenient to introduce a one-to-one conformal map from a canonical doubly-connected region in a parametric ζ-plane. Such a region is given by the annulus $\rho < |\zeta| < 1$ shown in Figure 2; ρ is known as the conformal modulus [24, pp. 333-334]. The existence of a conformal mapping from some such annulus to the fluid domain is guaranteed by the Riemann mapping theorem; ρ must be computed as part of the solution. The circle $|\zeta| = 1$ maps to the boundary of bubble 1, while the circle $|\zeta| = \rho$ maps to the boundary of bubble 2. The conformal map must have a simple pole in the annulus $\rho < |\zeta| < 1$ corresponding to the point mapping to infinity in the physical z-plane. It must also be such that z_ζ vanishes nowhere in $\rho < |\zeta| < 1$. This is a necessary, but not sufficient, condition for $z(\zeta)$ to be a one-to-one mapping.

If $W(z, \bar{z}) = 0$ on bubble 1, this implies that, on $|\zeta| = 1$,

$$\bar{z}(\zeta^{-1}) f(z(\zeta)) + g(z(\zeta)) = 0, \tag{21}$$

where we have used that fact that $\bar{\zeta} = \zeta^{-1}$ on $|\zeta| = 1$. The fact that $W = 0$ on bubble 2 similarly implies that on $|\zeta| = \rho$,

$$\bar{z}(\rho^2 \zeta^{-1}) f(z(\zeta)) + g(z(\zeta)) = 0, \tag{22}$$

since $\bar{\zeta} = \rho^2 \zeta^{-1}$ on $|\zeta| = \rho$. Equations (21) and (22) constitute relations between functions of a single complex variable ζ so that, by the principle of analytic continuation, (21) also holds off the circle $|\zeta| = 1$, and (22) holds off $|\zeta| = \rho$. Assuming that both relations hold in an overlapping region inside the annulus $\rho < |\zeta| < 1$, then in order for the two equations to be mutually compatible, $z(\zeta)$ must be such that

$$\bar{z}(\rho^2 \zeta^{-1}) = \bar{z}(\zeta^{-1}). \tag{23}$$

Thus, in addition to the symmetry requirements already stated, (23) represents a further constraint on the relevant conformal mapping.

The following two special functions will be useful. Define $P_N(\zeta, \rho)$ and $Q_N(\zeta, \rho)$ via the infinite product expansions

$$P_N(\zeta, \rho) = (1 - \zeta^N) \prod_{k=1}^{\infty} (1 - \rho^{2kN} \zeta^N)(1 - \rho^{2kN} / \zeta^N), \tag{24}$$

and

$$Q_N(\zeta, \rho) = (1 + \zeta^N) \prod_{k=1}^{\infty} (1 + \rho^{2kN} \zeta^N)(1 + \rho^{2kN} / \zeta^N). \tag{25}$$

These functions are related to the standard theta functions [25, Chapter 16]. Simple manipulation of the infinite product definitions show that they satisfy the following functional equations;

$$\begin{aligned} P_N(\zeta^{-1}, \rho) &= P_N(\rho^2 \zeta, \rho) = -\frac{1}{\zeta^N} P_N(\zeta, \rho); \\ Q_N(\zeta^{-1}, \rho) &= Q_N(\rho^2 \zeta, \rho) = \frac{1}{\zeta^N} Q_N(\zeta, \rho). \end{aligned} \tag{26}$$

A class of conformal maps that will be shown to give solutions of the physical problem considered is

$$z(\zeta) = \frac{P_1(-\zeta\sqrt{\rho}^{-1}, \rho)}{P_1(\zeta\sqrt{\rho}^{-1}, \rho)} \left(A\frac{Q_2(\zeta\sqrt{\rho}, \rho)}{P_2(\zeta\sqrt{\rho}, \rho)} + B\frac{P_1(-\zeta\sqrt{\rho}, \rho)}{P_1(\zeta\sqrt{\rho}, \rho)} \right), \tag{27}$$

where ρ, A and B are real parameters. First note that $\zeta = \sqrt{\rho}$ maps to infinity in the physical plane, while $\zeta = -\sqrt{\rho}$ maps to $z = 0$. (27) is also seen to satisfy

$$\overline{z}(\zeta) = z(\zeta). \tag{28}$$

This implies that the bubble configuration is symmetric with respect to reflection in the real z-axis. To see this, suppose $z_* = z(\zeta_*)$ is a point on the boundary of bubble 1. Then,

$$\overline{z}_* = \bar{z}(\bar{\zeta}_*) = z(\bar{\zeta}_*). \tag{29}$$

But because $\bar{\zeta}_*$ is also on the unit ζ-circle, $\bar{z}_* = z(\bar{\zeta}_*)$ is *also* a point on bubble 1 and is the reflection of z_* in the real axis. This is true for all choices of z_*, which implies that the bubble configuration is refectionally-symmetric with respect to the real axis.

Next, use of properties (26) show that, under the transformation $\zeta \mapsto \hat{\zeta} = \rho/\zeta$ (which takes a point on the circle $|\zeta| = 1$ to a point on the circle $|\zeta| = \rho$), the conformal map satisfies

$$z(\hat{\zeta}) = -z(\zeta). \tag{30}$$

This implies that each point on bubble 2 corresponds to a rotation by an angle of π of a point on bubble 1. Finally, the properties (26) can be used to verify that the map (27) satisfies the functional relation

$$z(\rho^2\zeta) = z(\zeta) \tag{31}$$

for all $\zeta \neq 0$. In particular, combining (31) with (28) shows that the map (27) satisfies the required condition (23).

Inspection reveals that the conformal map (27) has an infinite number of simple poles in the complex plane and is therefore not a rational function as in the case of the exact single bubble solutions [10], [11]. Note, however, that, once the singularities in $\rho < |\zeta| < \rho^{-1}$ are specified, the positions and strengths of all other singularities in the complex plane are determined by the multiplicative periodicity condition (31). It is therefore sufficient to consider the singularity structure of the conformal map in the annulus $\rho < |\zeta| < \rho^{-1}$. Figure 3 shows the distribution of simple pole singularities of the map (27) inside this annulus.

Using conditions (5) and the relations

$$z_s = \frac{i\zeta z_\zeta}{|z_\zeta|} \quad \text{on } |\zeta| = 1, \tag{32}$$

and

$$z_s = -\frac{i\zeta z_\zeta}{\rho|z_\zeta|} \quad \text{on } |\zeta| = \rho, \tag{33}$$

we may write the kinematic condition (9) as follows

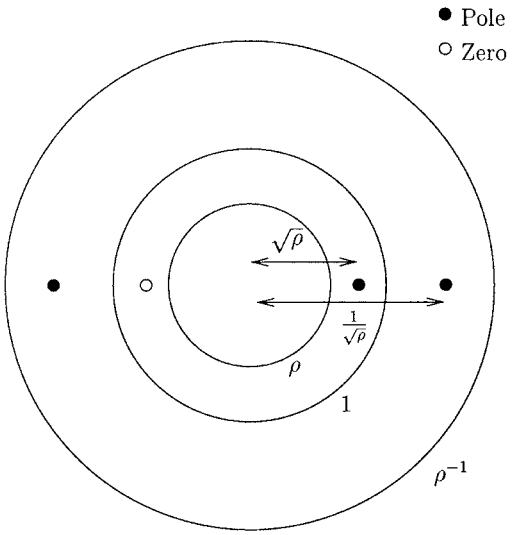

Figure 3. Singularities of the conformal map (27) in the annulus $\rho < |\zeta| < \rho^{-1}$. All poles shown are simple poles. The point $\zeta = \sqrt{\rho}$ maps to physical infinity while $\zeta = -\sqrt{\rho}$ maps to the physical origin. The circles $|\zeta| = 1$ and $|\zeta| = \rho$ map to the two boundaries of the bubbles.

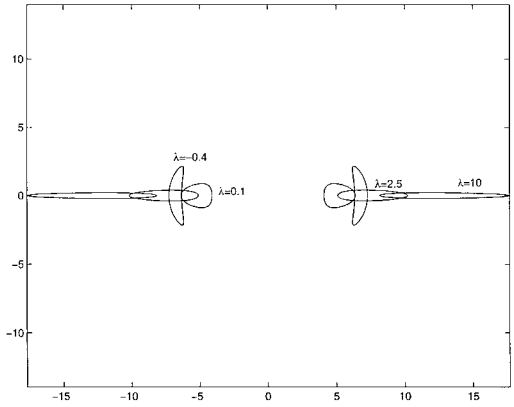

Figure 4. Equilibrium bubble shapes for fixed $\rho = 0{\cdot}01$ and various values of λ. The dimensionless area of all bubbles is π.

$$\mathfrak{Re}\left[\frac{2f(z(\zeta))}{\zeta z_\zeta}\right] = \begin{cases} \dfrac{1}{2}|z_\zeta|^{-1} & \text{on } |\zeta| = 1 \\ -\dfrac{1}{2}\rho|z_\zeta|^{-1} & \text{on } |\zeta| = \rho. \end{cases} \tag{34}$$

From (12) it is known that, to within multiplicative constants, $f(z) \sim z^3$ while $z_\zeta \sim z^2$ as $z \to \infty$. This implies that the term inside the square brackets in (34), when considered as a function of ζ, has a simple pole at $\zeta = \sqrt{\rho}$. Now, introduce an auxiliary function $q(\zeta)$ defined as

$$q(\zeta) = \frac{P_1(-\zeta\rho^{-1/2};\rho)P_1(-\zeta^{-1}\rho^{-1/2};\rho)}{P_1(\zeta\rho^{-1/2};\rho)P_1(\zeta^{-1}\rho^{-1/2};\rho)}. \tag{35}$$

This function has a simple pole at $\zeta = \sqrt{\rho}$. It also satisfies

$$q(\zeta) = q(\zeta^{-1}) = q(\rho^2\zeta) \tag{36}$$

Subtracting $\mathfrak{Re}[F_0 q(\zeta)]$ from (34), where F_0 is some real constant to be determined, we have

$$\mathfrak{Re}\left[\frac{2f(z)}{\zeta z_\zeta} - F_0 q(\zeta)\right] = \begin{cases} \dfrac{1}{2}|z_\zeta|^{-1} - \mathfrak{Re}[F_0 q(\zeta)] & \text{on } |\zeta| = 1 \\ -\dfrac{1}{2\rho}|z_\zeta|^{-1} - \mathfrak{Re}[F_0 q(\zeta)] & \text{on } |\zeta| = \rho. \end{cases} \tag{37}$$

For a suitable value of F_0, the term in the square brackets in (37) will be analytic and single-valued in the annulus $\rho < |\zeta| < 1$. In order to obtain the required single-valuedness, F_0 must satisfy

$$\oint_{|\zeta|=1}\left(\frac{1}{2|z_\zeta|}-\mathfrak{Re}[F_0q(\zeta)]\right)\frac{\mathrm{d}\zeta}{\zeta}=\oint_{|\zeta|=\rho}\left(-\frac{1}{2\rho|z_\zeta|}-\mathfrak{Re}[F_0q(\zeta)]\right)\frac{\mathrm{d}\zeta}{\zeta}. \tag{38}$$

It can be shown from (36) that $q(\zeta)$ is real on $|\zeta|=1$ and $|\zeta|=\rho$. Thus, F_0 satisfies

$$F_0\oint_{C_0}q(\zeta)\frac{\mathrm{d}\zeta}{\zeta}=\oint_{|\zeta|=1}\frac{1}{2|z_\zeta|}\frac{\mathrm{d}\zeta}{\zeta}+\oint_{|\zeta|=\rho}\frac{1}{2\rho|z_\zeta|}\frac{\mathrm{d}\zeta}{\zeta}. \tag{39}$$

Using the residue theorem, we obtain the following explicit formula for F_0,

$$F_0=\frac{\hat{P}_1(1,\rho)P_1(\rho^{-1},\rho)}{P_1(-1,\rho)P_1(-\rho^{-1},\rho)}\left[\frac{1}{2\pi\mathrm{i}}\oint_{|\zeta|=1}\frac{1}{2|z_\zeta|}\frac{\mathrm{d}\zeta}{\zeta}+\oint_{|\zeta|=\rho}\frac{1}{2\rho|z_\zeta|}\frac{\mathrm{d}\zeta}{\zeta}\right], \tag{40}$$

where the function $\hat{P}_N(\zeta,\rho)$ is defined by

$$\hat{P}_N(\zeta,\rho)\equiv\frac{P_N(\zeta,\rho)}{(1-\zeta^N)}=\prod_{k=1}^{\infty}(1-\rho^{2kN}\zeta^N)(1-\rho^{2kN}/\zeta^N). \tag{41}$$

With F_0 given by (40), the Villat formula [26, pp. 227–230] for an annulus (which gives an integral expression for a function analytic in an annulus given its real part on the two boundary circles) provides the following expression for $f(z(\zeta))$,

$$2f(z(\zeta))=[I(\zeta)+F_0q(\zeta)]\zeta z_\zeta(\zeta), \tag{42}$$

where $I(\zeta)$ is defined as

$$I(\zeta)=I^+(\zeta)-I^-(\zeta)+I_c, \tag{43}$$

with the functions $I^+(\zeta)$ and $I^-(\zeta)$ defined by

$$I^+(\zeta)=\frac{1}{2\pi\mathrm{i}}\oint_{|\zeta'|=1}\frac{\mathrm{d}\zeta'}{\zeta'}\left(1-2\frac{\zeta}{\zeta'}\frac{P_{1\zeta}(\frac{\zeta}{\zeta'},\rho)}{P_1(\frac{\zeta}{\zeta'},\rho)}\right)\left[\frac{1}{2|z_\zeta(\zeta')|}-F_0q(\zeta')\right], \tag{44}$$

$$I^-(\zeta)=\frac{1}{2\pi\mathrm{i}}\oint_{|\zeta'|=\rho}\frac{\mathrm{d}\zeta'}{\zeta'}\left(1-2\frac{\zeta}{\zeta'}\frac{P_{1\zeta}(\frac{\zeta}{\zeta'},\rho)}{P_1(\frac{\zeta}{\zeta'},\rho)}\right)\left[-\frac{1}{2\rho|z_\zeta(\zeta')|}-F_0q(\zeta')\right], \tag{45}$$

and the constant I_c is given by

$$I_c=-\frac{1}{2\pi\mathrm{i}}\oint_{|\zeta|=\rho}\frac{\mathrm{d}\zeta}{\zeta}\left[-\frac{1}{2\rho|z_\zeta(\zeta)|}-F_0q(\zeta)\right]. \tag{46}$$

$P_{1\zeta}(\zeta,\rho)$ denotes the partial derivative of the function $P_1(\zeta,\rho)$ with respect to its first argument.

Equation (42) determines the Goursat function $f(z(\zeta))$ in terms of the geometrical configuration encoded in the conformal mapping $z(\zeta)$. The remaining Goursat function $g(z(\zeta))$ now follows from either (21) or (22), *i.e.*,

$$g(z(\zeta))=-\bar{z}(\zeta^{-1})f(z(\zeta)). \tag{47}$$

It is important to examine the singularities of the function $g(z(\zeta))$ as given by (47) inside the fluid domain in order to ensure that it has the required analyticity properties there. Expression (47) involves the function $\bar{z}(\zeta^{-1})$ which has singularities at $\zeta = \sqrt{\rho}$ (corresponding to $z \to \infty$) and at $\zeta = -\sqrt{\rho}$ (corresponding to the physical origin). This is clearly seen from Figure 3 where the $\zeta \mapsto \zeta^{-1}$ inversion of the argument of the conjugate conformal map maps the two singularities of $z(\zeta)$ at $\zeta = \pm 1/\sqrt{\rho}$ into the annulus $\rho < |\zeta| < 1$ corresponding to the fluid region (recall from (28) that here the conjugate conformal-mapping function is precisely the conformal map itself). These two singularities are now considered individually. First, to within multiplicative constants, $\bar{z}(\zeta^{-1}) \sim 1/(\zeta - \sqrt{\rho}^{-1}$ as $\zeta \to \sqrt{\rho}$, while $f(z(\zeta)) \sim 1/(\zeta - \sqrt{\rho})^{-3}$ as $\zeta \to \sqrt{\rho}$ so that, by (47), $g(z(\zeta)) \sim 1/(\zeta - \sqrt{\rho})^{-4}$. This implies that $g(z) \sim g_4 z^4$ (for some g_4) as $z \to \infty$ as required in (12). Next, because $\bar{z}(\zeta^{-1})$ has a simple pole at $\zeta = -\sqrt{\rho}$, in order that $g(z(\zeta))$ is analytic at the physical origin, we must ensure that $f(z(\zeta))$ vanishes at $z = 0$ (or $\zeta = -\sqrt{\rho}$) in order to remove the singularity of $\bar{z}(\zeta^{-1})$. But the condition $f(0) = 0$ is forced by the symmetry of the problem and the fact that the physical origin must be a stagnation point of the flow. Mathematically, from (42) and because $q(-\sqrt{\rho}) = 0$, this condition is equivalent to

$$I(-\sqrt{\rho}) = 0 \tag{48}$$

– a fact that can be checked *a posteriori* by numerical evaluation of the integrals involved in the definition of $I(\zeta)$ given in (46)–(46).

In summary, we have now explicitly constructed the two Goursat functions $f(z)$ and $g(z)$ in terms of the conformal mapping variable ζ with all the required analyticity properties. The conformal maps (27) therefore represent exact solutions describing the shapes of two symmetric bubbles in equilibrium embedded in a flow with the far-field behaviour given in (12).

The conformal map (27) contains three real parameters ρ, A and B. The pressure inside each bubble has been assumed equal to zero. If we assume that the area of each bubble is specified, it is to be expected that the value of f_1 will be implicitly determined (if the flow was such that the fluid pressure at infinity tended to a constant, f_1 would be proportional to this constant). The area condition represents one condition relating the parameters ρ, A and B. Two additional conditions are obtained by ensuring that $f(z) \sim f_3 z^3 + \mathcal{O}(z)$ as $z \to \infty$ and that $g(z) \sim g_4 z^4 + \mathcal{O}(z^2)$ as $z \to \infty$ where f_3 and g_4 are externally specified. Thus for given bubble area and given f_3 and g_4, the direct problem is to solve for the corresponding conformal mapping parameters ρ, A and B. Alternatively, having specified ρ, A and B corresponding to a univalent map, the inverse problem is solved by computing the corresponding values of the bubble area, f_3 and g_4.

It is important to make clear a distinction from the single bubble analysis of Antanovskii [10], [11]. In that work, it proved possible to construct a rational conformal mapping function from the circular disk $|\zeta| < 1$ to the fluid region exterior to the bubble corresponding to any given bubble area, g_4, f_3 and g_2. In the two bubble case, it appears that once the bubble area and the values of g_4 and f_3 are specified, the value of g_2 giving rise to equilibrium is determined by the solution. It may be that a more general class of solutions exists which will allow g_2 to be independently specified but the present author has not succeeded in identifying such a class. Whether a more general class of two-bubble equilibria exists remains an open question at present.

A consistency check on the solutions is obtained by expanding $f(z)$ and $g(z)$ in powers of z as $z \to \infty$. After due manipulations, expressions for the coefficient of z^2 in the expansion

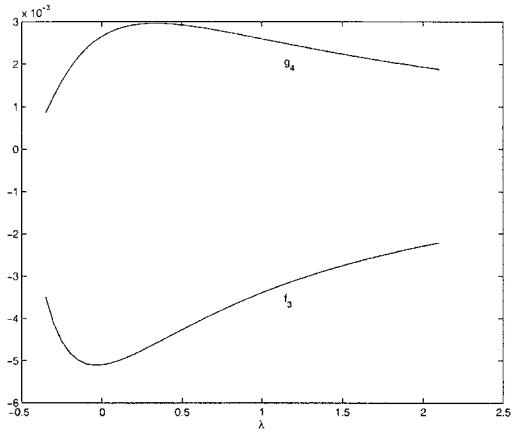

Figure 5. Values of g_4 and f_3 against λ for fixed $\rho = 0{\cdot}01$ and bubble area equal to π.

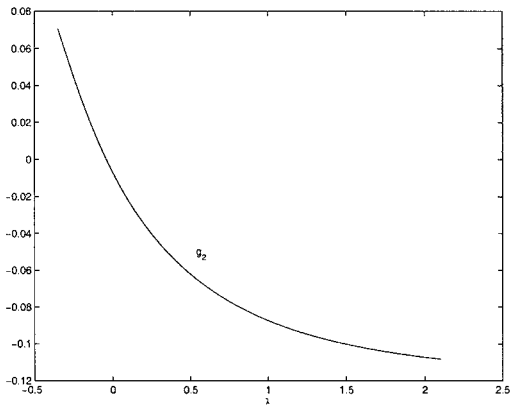

Figure 6. Values of g_2 against λ for fixed $\rho = 0{\cdot}01$ and bubble area equal to π.

of $f(z)$ and for the coefficient of z^3 in the expansion of $g(z)$ can be deduced. These should be zero and this can be checked numerically. Appendix A gives more explicit details of these consistency conditions, including a derivation of the far-field equations relating the conformal mapping parameters $\{\rho, A, B\}$ to the flow characteristics, *i.e.*, g_4, f_3, g_2 and the bubble area.

Although the Goursat functions have been given explicitly, the formulae involve integrals that cannot be evaluated in closed form. Numerical quadrature is needed to evaluate them. The solutions as well as the kernel of the integral function $I(\zeta)$ depend on the functions $P_N(\zeta, \rho)$ and $Q_N(\zeta, \rho)$ which have been defined in terms of an infinite product expansion. To perform the computations, expansions (24) and (25) are truncated at $k = 10$ terms which gives excellent accuracy. A check on this accuracy is performed by verifying that the conformal map satisfies the required property (23) for arbitrary choices of ζ. The integral function $I(\zeta)$ can be computed using a trapezoidal rule with super-algebraic convergence for the present periodic functions on periodic domains.

6. Investigation of bubble shapes

Rather than seeking solutions for given f_3, g_4 and bubble area, we have chosen instead to investigate the class of conformal maps (27) for different values of the parameters ρ, A and B. In this way, possible equilibrium bubble shapes can be systematically surveyed.

Some preliminary observations are made. First, for fixed choices of A and B, it is found that the two bubbles move further apart as $\rho \to 0$. In a general sense, ρ can therefore be viewed as representing a measure of the separation of the two bubbles with small values of ρ corresponding to widely-separated bubbles. Second, univalent mappings can only be constructed provided ρ is sufficiently small, *i.e.*, the space of parameters (A, B) for which univalent maps exist is found to get smaller with increasing ρ. The procedure adopted to investigate the solutions is as follows: a value of ρ is fixed; different values of the ratio $\lambda \equiv B/A$ are then explored with A determined by the condition that the (non-dimensional) area of each bubble is equal to π; the corresponding values of g_4, g_2 and f_3 are then calculated *a posteriori*.

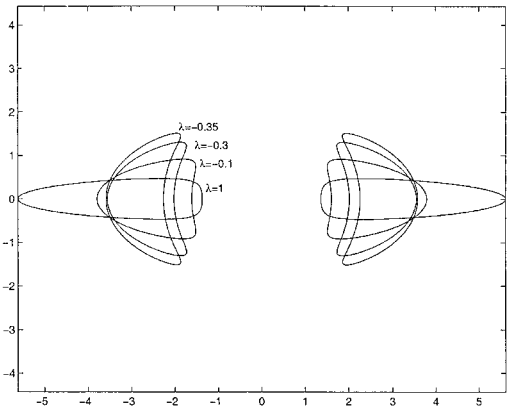

Figure 7. Equilibrium bubble shapes for fixed $\rho = 0{\cdot}05$ and various values of λ. The area of all bubbles is π.

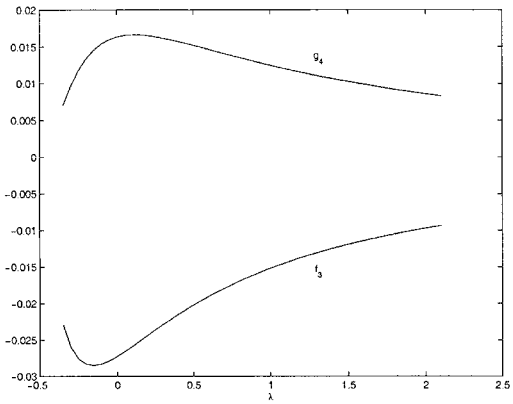

Figure 8. Values of g_4 and f_3 against λ for fixed $\rho = 0{\cdot}05$ and bubble area equal to π.

First we examine how the bubble shapes depend on the two parameters ρ and λ. Figure 4 shows the case of $\rho = 0{\cdot}01$ for various choices of λ. The bubble shapes for different λ are superposed on the same diagram, but the far-field conditions in each case are different. The corresponding values of g_4, f_3 and g_2 can be read from the graphs featured in Figures 5 and 6 which show plots of these parameters for fixed $\rho = 0{\cdot}01$ and bubble area equal to π, as functions of the parameter λ. In a similar way, for $\rho = 0{\cdot}05$ superposed bubble shapes for different λ-values are shown in Figure 7 with corresponding far-field asymptotic flow conditions graphed in Figures 8 and 9. Figures 10–11 show analogous results for $\rho = 0{\cdot}1$. Note the general trend, consistent with the observation made above, that for higher values of ρ the bubbles are closer together on the whole. This can be seen by comparing Figures 4, 7 and 10 which correspond to successively larger values of ρ. In each case with ρ fixed, it is found that there exists a lower limit, $\lambda = \lambda_c$ say, for which a univalent mapping from the annulus can be found. For example, in the case $\rho = 0{\cdot}01$, $\lambda_c \approx -0{\cdot}49$. For all examples calculated, λ_c is found to be negative and to increase with increasing ρ. As $\lambda \to \lambda_c$ for fixed ρ, each bubble develops two pointed vertical ends having high curvature and, for the higher ρ-values when the bubbles are generally closer together, these two points of high curvature on the separate bubbles in the first and second quadrant draw close together (with a reflectionally-symmetric situation occurring in the third and fourth quadrants). In the limit $\lambda \to \lambda_c$, these high curvature points appear to become near-cuspidal, especially for the larger ρ-values. The appearance of near-cusps in free boundaries involving slow viscous flows is by now well known (*e.g.* [27], [19], [20]). It is found that, as the bubbles draw closer together, their interaction with both each other and the ambient flow induces the formation of both a concave ('dimple') region. For lower values of ρ (so that the bubbles are, on the whole, more widely separated) these concave regions and the points of high curvature are less pronounced and the bubbles have generally smoother shapes. The dimple regions are most apparent in Figure 10. The phenomenon of 'dimpling' is well-known in studies of droplet coalescence and film drainage [1, 28, 18] and are a consequence of the pressure gradients associated with the bubbles drawing closer together.

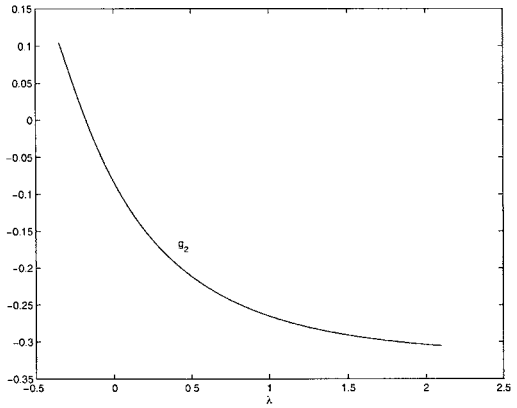

Figure 9. Values of g_2 against λ for fixed $\rho = 0{\cdot}05$ and bubble area equal to π.

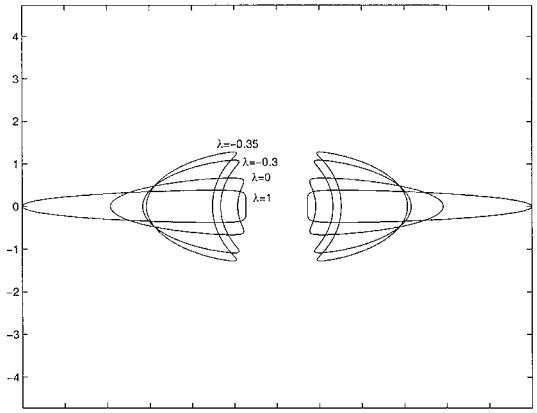

Figure 10. Equilibrium bubble shapes for fixed $\rho = 0{\cdot}1$ and various values of λ. The area of all bubbles is π.

Typically, as ρ gets larger, bubble shapes obtain larger aspect ratios, the bubbles get closer together and the dimples become increasingly semi-circular in shape. This can lead to configurations in which the two bubbles almost touch at the near-cusps and enclose a near-circular region of fluid thereby forming what resembles a single composite bubble containing a stagnant circular droplet. This limiting situation is reminiscent of the limiting states for isolated bubbles in an ambient parabolic flow as calculated by Richardson [5]. There, the rear of the bubble develops a re-entrant wake which, in the limiting case, displays two points of high curvature which draw together to enclose a circular region of near-stagnant fluid. A near-limiting configuration in the two-bubble case is given in Figure 13 where $\rho = 0{\cdot}4$ (a value quite close to the upper limit for which univalent mappings of this kind exist) and $\lambda = -0{\cdot}25$. Figure 13 should be compared to Figure 3(f) of Richardson [5].

On the other hand, as λ increases for fixed ρ, the aspect ratio of the bubbles increases and the distance between the bubbles tends to decrease. In the case of sufficiently small ρ, there appears to be an intermediate value of λ at which the distance of closest approach of the two bubbles ceases to decrease and instead gets larger (see Figures 4 and 7). All the time, as λ increases, the aspect ratio of the bubbles continues to increase. Steady solutions appear to exist for all positive values of λ, the aspect ratio growing very large as $\lambda \to \infty$. Figure 14 shows bubble shapes in the case $\rho = 0{\cdot}05$ for λ near to λ_c and also for a large, positive λ-value ($\lambda = 5$). This figure illustrates the typical extremes of the possible equilibrium bubble shapes for a fixed ρ-value.

The value of f_3 is found to be negative whatever values are taken for the parameters appearing in the conformal map (27). This is significant because Antanovskii [10], [11] found that the sign of a 'pressure parameter' (which is related to the sign of the cubic terms in $f(z)$) is crucial in determining whether a single bubble will 'cusp' or 'burst'. To make a closer connection with the single-bubble analysis of Antanovskii [10], note first that Antanovskii's choice of non-dimensionalization is different to that adopted here. In particular, Antanovskii rescales time with respect to a local deformation rate G of the ambient velocity field as opposed to the $a_0\mu/\sigma$ used here. However, for present purposes we are concerned only with

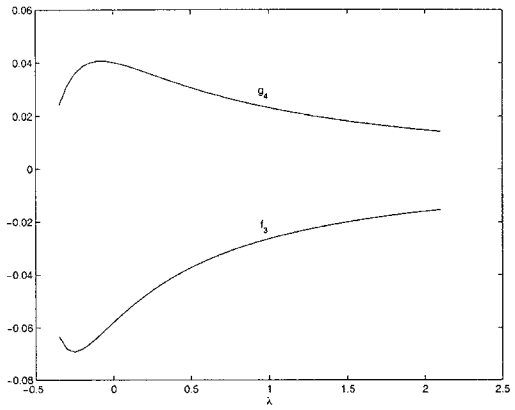

Figure 11. Graph of values of g_4 and f_3 against λ for fixed $\rho = 0{\cdot}1$ and bubble area equal to π.

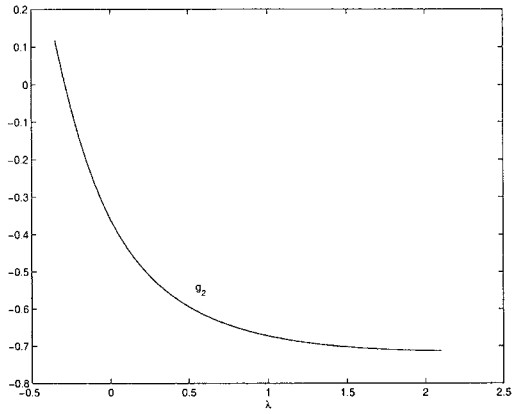

Figure 12. Graph of values of g_2 against λ for fixed $\rho = 0{\cdot}1$ and bubble area equal to π.

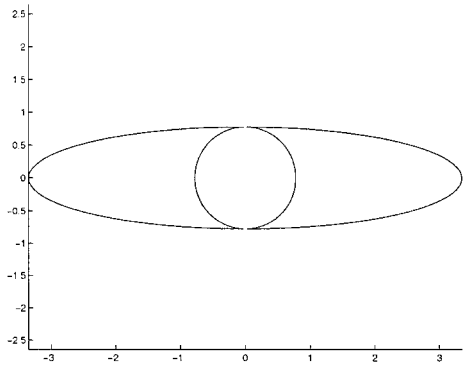

Figure 13. Bubble shapes for $\rho = 0{\cdot}4$ and $\lambda = -0{\cdot}25$. The near-cuspidal points on the two bubbles almost touch thus enclosing a near-circular region of fluid.

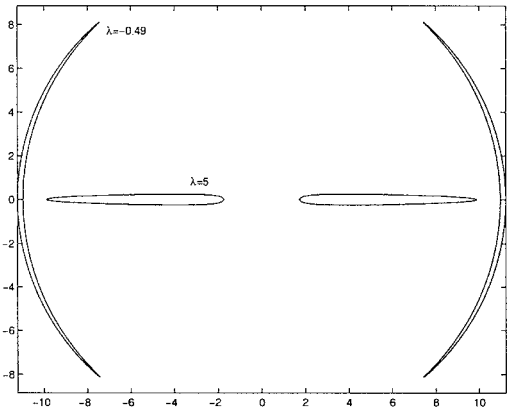

Figure 14. Near-limiting bubble shapes for fixed $\rho = 0{\cdot}05$. For $\lambda \approx -0{\cdot}49$ the bubbles become elongated in the vertical direction and develop near-cusps at the top and bottom. As λ becomes large and positive (here $\lambda = 5$) the bubbles are drawn out horizontally. The area of all bubbles is π.

the signs of various quantities. To within positive constants, the correspondence between the dimensionless parameters a, b and G used in [10] and the parameters f_3, g_4 and g_2 used here is the following:

$$f_3 \sim Gb, \qquad g_4 \sim Ga, \qquad g_2 \sim G \tag{49}$$

Antanovskii takes G positive and, in cases $a \leq 0$ or $b \leq 0$, he essentially finds that there is an upper bound on G for which a steady solution exists. He associates this upper bound on the existence of solutions with the onset of bursting of the single bubble. Antanovskii's results are consistent with the new solutions found here; observe from Figures 6, 9 and 12 that as $\lambda \to \lambda_c$ (the quantity λ can be identified with Antanovskii's deformation parameter q) the

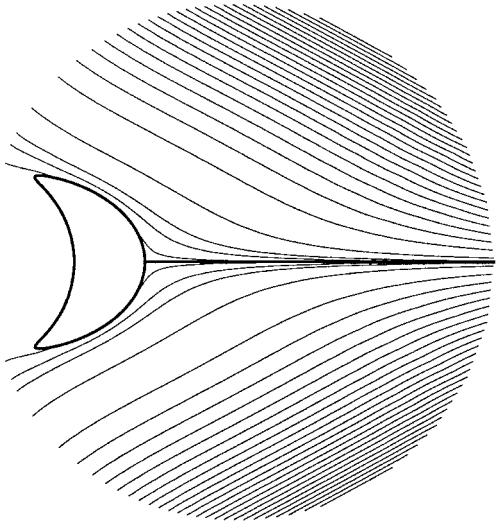

Figure 15. Streamlines around one of the two bubbles for parameter values $\rho = 0{\cdot}1$ and $\lambda = -0{\cdot}4$. The far-field streamlines resemble those of a stagnation point flow about the origin.

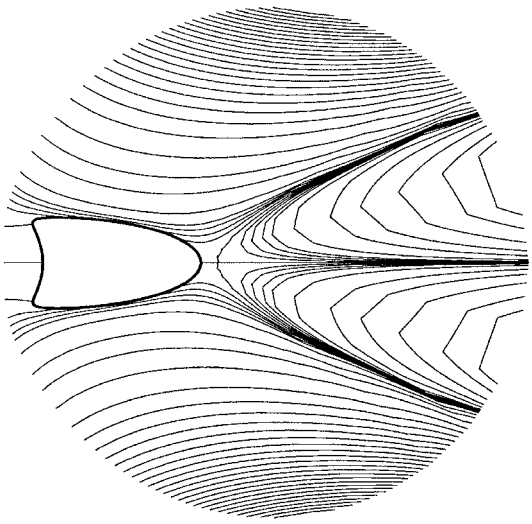

Figure 16. Streamlines for parameter values $\rho = 0{\cdot}1$ and $\lambda = -0{\cdot}1$. The $\psi = 0$ contour is now seen to form a separatrix streamline between distinct parts of the flow.

quantity g_2 increases to a maximum positive value. Because solutions with λ close to λ_c have an associated g_2 which is positive and f_3 negative, the identifications in (49) show that the far-field flow in which such two-bubble solutions find themselves correspond to the $b < 0$ far-field flows of Antanovskii. These are precisely the far-field flows which Antanovskii associates with the 'bursting' of a single bubble. It is therefore tempting to suggest that the new two-bubble configurations with λ close to λ_c might constitute equilibria to which a 'burst' bubble will relax when it can no longer exist as a single entity. It is also worth pointing out that the 'single' composite bubble in Figure 13 discussed above (containing, in the limit, a stagnant circular blob of fluid) to which the close-to-limiting two-bubble configuration seems to converge, has a shape highly reminiscent of the $b < 0$ single-bubble solutions (*i.e.*, 'bursting' solutions) displayed in Figures 5 and 6 of Antanovskii [10].

Finally, to gain a better understanding of the nature of the ambient flow-field, it is instructive to plot the associated streamline patterns. An explicit formula for the streamfunction ψ as a function of ζ and $\bar{\zeta}$ is given by

$$\psi(\zeta, \bar{\zeta}) = \mathfrak{Im}\left[\left(\bar{z}(\bar{\zeta}) - \bar{z}(\zeta^{-1})\right) f(z(\zeta))\right], \tag{50}$$

where $f(z(\zeta))$ is given explicitly in (42). This formula can be used to plot ψ-contours which are the streamlines. If required, the pressure field can also be computed in a straightforward way using the formula

$$p = \mathfrak{Re}\left[\frac{4}{z_\zeta(\zeta)}\frac{\mathrm{d}f(z(\zeta))}{\mathrm{d}\zeta}\right]. \tag{51}$$

Figures 15–17 depict typical streamlines around one of the two bubbles for fixed $\rho = 0{\cdot}1$ and three different choices of $\lambda = -0{\cdot}4, -0{\cdot}1$ and 1 (the streamline distribution around the other bubble being obvious from symmetry). The dimensionless area of the bubble in each

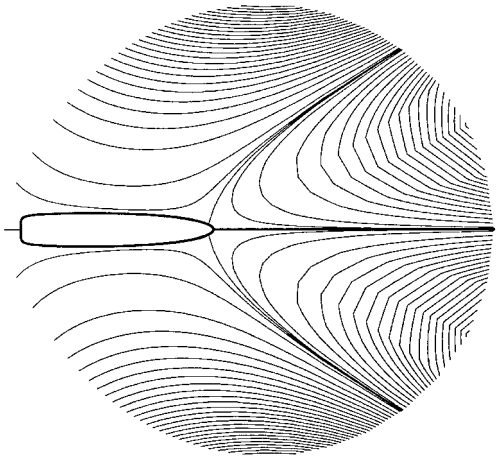

Figure 17. Streamlines for parameter values $\rho = 0{\cdot}1$ and $\lambda = 1$. At this value of the parameters, the $\psi = 0$ separatrix streamline has now met with the bubble (which is also a $\psi = 0$ contour).

case is π. These figures illustrate how the topology of the streamline distribution changes as λ increases for fixed ρ. In Figure 15, the streamline pattern resembles that of a stagnation point flow about the origin. As λ increases, the nature of the streamline pattern changes. In Figure 16 the $\psi = 0$ streamline is seen to form a separatrix between distinct regions of the flow behind the bubble. As λ increases further, this separatrix streamline reaches the bubble and bifurcates along the top and bottom, as seen in Figure 17.

7. Discussion

It would be interesting to examine experimentally to what degree any of the computed bubble shapes might be reproduced in an appropriately-configured four-roller mill using clean low-viscosity fluids. It is worth remembering that the two-dimensional single-bubble model considered by Antanovskii [11] shows remarkably similar bubble profiles to cross-sections of the fully three-dimensional bubbles observed experimentally by Taylor [17]. The bubbles considered here are assumed to be inviscid and at constant internal pressure with free boundaries that are free of surfactants. This leads to a situation in which the interfaces are highly mobile; introducing a non-zero viscosity and hydrodynamic coupling with the bubble phase or surfactants on the bubble boundaries is generally expected to reduce this mobility and thereby reduce the deformability of the interfaces. Some of the more deformed bubble shapes observed in the present study are not therefore expected to be observable in experiments involving real fluids. In particular, while qualitatively consistent with prior observations, some of the 'dimple' regions observed are very much more pronounced than that seen in, for example, studies of droplet coalescence [28, 29] or studies of bubbles approaching walls [30]. These pronounced shapes are partly due to the high mobility of the bubble interfaces in the present model.

The stability of the equilibrium solutions is of interest but lies beyond the scope of the present paper. More generally, the problem of two time-evolving interacting bubbles also remains to be investigated. Such an investigation can be performed numerically (*e.g.*, using boundary-integral methods for which the present exact solution class may provide valuable checks on the code) but the existence of exact solutions for time-evolving bubbles in the

single-bubble case suggests the possibility that the exact results here might similarly be generalizable to a quasi-steady, time-evolving class of exact solutions in which the parameters appearing in the conformal-mapping functions evolve according to some (finite) nonlinear system of differential equations as in the single bubble case [8, 9, 22]. Any developments of this kind would provide a useful theoretical framework for studying the two-droplet coalescence problem [18], albeit in a planar model.

The exact solutions suggest further possibilities for generalizations in other directions. There is, in principle, no obstruction to extending the present steady analysis to bubbles with surfactants and such generalizations in the single-bubble case have been performed by Siegel [31, 32] resulting in exact solutions for both the bubble shape, the associated flow and the steady surfactant distribution. The present author has also recently demonstrated [33] that the single-bubble exact solutions of Tanveer and Vasconcelos [8] can be generalized to the case of compressible bubbles whose pressure-area relation is governed by some externally specified equation of state – a scenario recently studied numerically by Pozrikidis [34]. Similar generalizations to compressible bubbles might also be feasible for two bubbles. Finally, derivation of exact solutions for equilibrium configurations involving multiple (*i.e.*, more than two) bubbles poses an intriguing challenge. It is hoped to explore these many various possibilities in future work.

Acknowledgements

The author acknowledges financial support from the Nuffield Foundation and from EPSRC grant GR/R40104/01.

Appendix, Derivation of the far-field equations

In this appendix, we indicate how to find relations between the conformal mapping parameters describing the bubble shapes and the parameters of the far-field asymptotic flow.

As $\zeta \to \sqrt{\rho}$, let

$$z(\zeta) \sim \frac{\alpha}{(\zeta - \sqrt{\rho})} + \beta + \gamma(\zeta - \sqrt{\rho}) + \dots , \tag{A1}$$

and

$$\bar{z}(\zeta^{-1}) \sim \frac{\delta}{(\zeta - \sqrt{\rho})} + \epsilon + \chi(\zeta - \sqrt{\rho}) + \dots , \tag{A2}$$

where expressions for $\alpha, \beta, \gamma, \delta, \epsilon$ and χ in terms of $\{\rho, A, B\}$ can be derived using (27). This is conveniently done with the help of a symbolic manipulator. We also let

$$F_0 q(\zeta) \sim \frac{q_{-1}}{(\zeta - \sqrt{\rho})} + q_0 + q_1(\zeta - \sqrt{\rho}) + \dots , \tag{A3}$$

as $\zeta \to \sqrt{\rho}$, where expressions for q_{-1}, q_0 and q_1 can be derived using (35) and (40). Using these expansions to expand $F(\zeta)$, as given in (42), as $\zeta \to \sqrt{\rho}$ we have

$$F(\zeta) \sim \frac{F_3}{(\zeta - \sqrt{\rho})^3} + \frac{F_2}{(\zeta - \sqrt{\rho})^2} + \frac{F_1}{(\zeta - \sqrt{\rho})} + \dots , \tag{A4}$$

where

$$\begin{aligned} F_3 &= -\frac{\alpha\sqrt{\rho}q_{-1}}{2}, \\ F_2 &= -\frac{\alpha}{2}\Big(q_{-1} + (q_0 + I_0)\sqrt{\rho}\Big), \\ F_1 &= \frac{\gamma\sqrt{\rho}q_{-1}}{2} - \frac{\alpha}{2}\Big(q_0 + I_0 + (q_1 + I_1)\sqrt{\rho}\Big), \end{aligned} \tag{A5}$$

where $I_0 = I(\sqrt{\rho})$ and $I_1 = I_\zeta(\sqrt{\rho})$. At the same time, using (A1) to expand $f_3 z^3 + f_1 z$ in powers of $(\zeta - \sqrt{\rho})$ as $\zeta \to \sqrt{\rho}$ gives

$$F(\zeta) \sim \frac{f_3\alpha^3}{(\zeta-\sqrt{\rho})^3} + \frac{3\alpha^2\beta f_3}{(\zeta-\sqrt{\rho})^2} + \frac{(f_1\alpha + f_3(3\alpha^2\gamma + 3\alpha\beta^2)}{(\zeta-\sqrt{\rho})} + \dots \tag{A6}$$

Equating coefficients of $(\zeta - \sqrt{\rho})^{-3}$ in (A4) and (A6) gives f_3 in terms of the conformal mapping parameters, *i.e.*,

$$f_3 = -\frac{\sqrt{\rho}q_{-1}}{2\alpha^2}, \tag{A7}$$

while the coefficient of $(\zeta - \sqrt{\rho})^{-2}$ provides the following consistency condition between the parameters,

$$3\beta\sqrt{\rho}q_{-1} = \alpha\Big(q_{-1} + (q_0 + I_0)\sqrt{\rho}\Big). \tag{A8}$$

That the solutions satisfy this condition can be confirmed numerically.

Similarly, expanding $G(\zeta)$ as given in (47) as $\zeta \to \sqrt{\rho}$ yields

$$G(\zeta) \sim -\frac{\delta F_3}{(\zeta-\sqrt{\rho})^4} - \frac{(\epsilon F_3 + \delta F_2)}{(\zeta-\sqrt{\rho})^3} - \frac{(\chi F_3 + \epsilon F_2 + \delta F_1)}{(\zeta-\sqrt{\rho})^2} + \dots, \tag{A9}$$

while, from (1), $g_4 z^4 + g_2 z^2$ has the behaviour

$$G(\zeta) \sim \frac{g_4\alpha^4}{(\zeta-\sqrt{\rho})^4} + \frac{4\alpha^3\beta g_4}{(\zeta-\sqrt{\rho})^3} + \frac{\alpha^2 g_2 + g_4(4\alpha^3\gamma + 6\alpha^2\beta^2)}{(\zeta-\sqrt{\rho})^2}. \tag{A10}$$

as $\zeta \to \sqrt{\rho}$. Equation coefficients in (A9) and (A10) provides the following expressions for g_4 and g_2 in terms of the conformal mapping parameters, *i.e.*,

$$g_4 = \frac{\delta\sqrt{\rho}q_{-1}}{2\alpha^3}, \tag{A11}$$

and

$$\begin{aligned} g_2 = \frac{\chi\sqrt{\rho}q_{-1}}{2\alpha} + \frac{\epsilon(q_{-1} + (q_0 + I_0)\sqrt{\rho})}{2\alpha} \quad & -\frac{\delta\gamma\sqrt{\rho}q_{-1}}{2\alpha^2} + \frac{\delta(q_0 + I_0 + \sqrt{\rho}(q_1 + I_1)}{2\alpha} \\ & -g_4(4\alpha\gamma + 6\beta^2), \end{aligned} \tag{A12}$$

as well as a consistency condition

$$4\sqrt{\rho}\beta\delta q_{-1} = \alpha\epsilon\sqrt{\rho}q_{-1} + \alpha\delta(q_{-1} + (q_0 + I_0)\sqrt{\rho}). \tag{A13}$$

Again, it can be checked numerically that the solutions satisfy (A13).

Finally, it is noted that the bubble area is given by the formula

$$-\Im\mathrm{m}\left[\frac{1}{2\mathrm{i}}\oint_{|\zeta|=1}\bar{z}(\zeta^{-1})z_\zeta(\zeta)\,\mathrm{d}\zeta - \frac{1}{2\mathrm{i}}\oint_{|\zeta|=\rho}\bar{z}(\rho^2\zeta^{-1})z_\zeta(\zeta)\,\mathrm{d}\zeta\right]. \tag{A14}$$

References

1. A.K. Chesters, The modelling of coalescence processes in fluid-liquid dispersions. *Chem. Eng. Res. Des.* 69 (1991) 259–270.
2. J.M. Rallison, The deformation of small viscous drops and bubbles in shear flows. *Ann. Rev. Fluid. Mech.* 16 (1984) 45–66.
3. H.A. Stone, Dynamics of drop deformation and breakup in viscous fluids. *Ann. Rev. Fluid. Mech.* 26 (1994) 65–102.
4. S. Richardson, Two-dimensional bubbles in slow viscous flows. *J. Fluid Mech.* 33 (1968) 475–493.
5. S. Richardson, Two-dimensional bubbles in slow viscous flows. Part 2. *J. Fluid Mech.* 58 (1973) 115–127.
6. R.W. Hopper, Plane Stokes flow driven by capillarity on a free surface. *J. Fluid Mech.* 213 (1990) 349–375.
7. R.W. Hopper, Plane Stokes flow driven by capillarity on a free surface, Part 2. Further developments. *J. Fluid Mech.* 230 (1991) 355–364.

8. S. Tanveer and G.L. Vasconcelos, Time-evolving bubbles in two dimensional Stokes flow. *J. Fluid Mech.* 301 (1995) 325–344.
9. L.K. Antanovskii, Quasi-steady deformation of a two-dimensional bubble placed within a potential viscous flow. *Eur. J. Mech. B/Fluids* 13 (1994) 73–92.
10. L.K. Antanovskii, A plane inviscid incompressible bubble placed within a creeping viscous flow: formation of a cusped bubble. *Eur. J. Mech. B* 13 (1994) 491–509.
11. L.K. Antanovskii, Formation of a pointed drop in Taylor's four-roller mill. *J. Fluid Mech.* 327 (1996) 325–341.
12. D.G. Crowdy and S. Tanveer, A theory of exact solutions for plane viscous blobs. *J. Nonlin. Sci.* 8 (1998) 261–279.
13. D.G. Crowdy and S. Tanveer, A theory of exact solutions for annular viscous blobs. *J. Nonlin. Sci.* 8 (1998) 375–400.
14. S. Richardson, Plane Stokes flow with time-dependent free boundaries in which the fluid occupies a doubly-connected region. *Eur. J. Appl. Math.* 11 (2000) 249–269.
15. D.G. Crowdy, Viscous sintering of unimodal and bimodal cylindrical packings with shrinking pores. *Eur. J. Appl. Math.* (2002) to appear.
16. D.G. Crowdy, Exact solutions for the viscous sintering of multiply-connected fluid domains. *J. Eng. Math.* 42 (2002) 225–242.
17. G.I. Taylor, The formation of emulsions in definable fields of flow. *Proc. R. Soc. London A* 146 (1934) 501–523.
18. H. Yang, C.C. Park, Y.T. Hu, L.G. Leal, The coalescence of two equal-sized drops in a two-dimensional linear flow. *Phys Fluids*, 13 (2001) 1087–1106.
19. C. Pozrikidis, Numerical studies of singularity formation at free surfaces and fluid interfaces in two-dimensional Stokes flow. *J. Fluid Mech.* 331 (1997) 145–167.
20. C. Pozrikidis, Numerical studies of cusp formation at fluid interfaces in Stokes flow. *J. Fluid Mech.* 357 (1998) 29–57.
21. M. Siegel, Cusp formation for time-evolving bubbles in two-dimensional Stokes flow, *J. Fluid Mech.* 412 (2000) 227–257.
22. D. Crowdy and M. Siegel, Exact solutions for the evolution of a bubble in Stokes flow: a Cauchy transform approach. *SIAM J. Appl. Math.* (2002) to appear.
23. W.E. Langlois, *Slow Viscous Flow*. New York: Macmillan (1964) 229 pp.
24. Z. Nehari, *Conformal Mapping*, New York: McGraw-Hill (1966) 396pp.
25. M. Abramovitz and I.A. Stegun, *Handbook of Mathematical Functions*. New York: Dover, (1972) 1046pp.
26. P. Henrici, *Applied and computational complex analysis*, Volume III. New York: Wiley and Sons (1986) 637pp.
27. J.T. Jeong and H.K. Moffatt, Free surface cusps associated with flow at low Reynolds number. *J. Fluid Mech.* 241 (1992) 1–22.
28. M.A. Rother, A.Z. Zinchenko and R.H. Davis, Buoyancy-driven coalescence of slightly deformable drops. *J. Fluid Mech.* 346 (1997) 117–148.
29. M. Loewenberg and E.J. Hinch, Collision of two deformable drops in shear flow. *J. Fluid Mech.* 338 (1997) 299–315.
30. C. Pozrikidis, The deformation of a liquid drop moving normal to a plane wall. *J. Fluid Mech.* 215 (1990) 331–363.
31. M. Siegel, Influence of surfactant on rounded and pointed bubbles in two-dimensional Stokes flow. *SIAM. J. Appl. Math.* 59 (1999) 1998–2027.
32. M. Siegel, Cusp formation for time-evolving bubbles in two-dimensional Stokes flow. *J. Fluid Mech.* 412 (2000) 227–257.
33. D.G. Crowdy, Compressible bubbles in Stokes flow. *J. Fluid Mech.* (to appear).
34. C. Pozrikidis, Expansion of a compressible gas bubble in Stokes flow. *J. Fluid Mech.* 442 (2001) 171–189.